Bonding performances of epoxy coatings reinforced by carbon nanotubes (CNTs) on mild steel substrate with different surface roughness

Dawei Zhang [a], Ying Huang [a]*, and Yechun Wang [b]

[a] *Department of Civil and Environmental Engineering, North Dakota State University, USA 58108*

[b] *Department of Mechanical Engineering, North Dakota State University, USA 58108*

**Corresponding author: Associate Professor, North Dakota State University, CIE201F, 1340 Administration Ave, Fargo, ND 58108, USA, Email: ying.huang@ndsu.edu; Phone: 701-231-7651; ORCID number: 0000-0003-4119-9522*

Abstract

This paper investigated the bonding performances of epoxy coatings reinforced by carbon nanotubes (CNTs) as additives on mild steel substrates. Pure epoxy and CNT-reinforced epoxy coatings on four different surface roughness of steel substrate were tested using single lap shear (SLS) tests. The SLS experimental results indicated that, on rougher substrates, the addition of a small percentage of CNTs (0.75% by weight) could significantly improve the bonding performance and change the failure mode from adhesion fracture to partly cohesive failure by improving the toughness of coatings and the interfacial adhesion between the coatings and substrates. In addition, the contact angle tests and the surface characterizations using scanning electron microscopy (SEM) analysis before and after fracture indicated that the wettability of coatings on steel substrates improved significantly with the increase of surface roughness and mechanical interlocking was the main reinforcing mechanism on rougher substrates.

Keywords: carbon nanotubes and nanofibers, resins, debonding, mechanical testing

1. Introduction

Polymeric coatings are one of the most commonly used coating types for protecting steel substrates from corrosion as a protective barrier and it has been extensively applied in civil and transportation industries such as underground, underwater and offshore infrastructures [1–3]. Epoxy resins, with high strength-to-weight ratio, good environmental stability and ease of application, have become a favorable polymeric coating material in the last few decades, especially for corrosion mitigation and prevention on pipeline and steel bridges. However, the weak bonding performance of the epoxy coatings on steel substrates [4,5] limited their long-term applications for effective and efficient corrosion protection in these fields since the debonding of the coatings could occur easily under external stresses [6]. The epoxy coatings have relatively weak bonding performance not only because they are brittle materials which yield relatively low ductility and resistance to crack propagations [7], but also given the fact that the steel and epoxy resins are dissimilar materials, the interfacial adhesion forces between steel and epoxy resins are mainly hydrogen and van der Waals force in the form of secondary bonding, which are weaker compared to adhesion between similar materials [8,9]. The brittleness of the pure epoxy resin results in the low bonding capacity of the coating due to poor mechanical properties [10], while the secondary bonding forces between the pure epoxy and steel substrate lead to premature adhesive failure in which the coating delaminates from the substrate before it fully deforms [11]. Therefore, to improve the bonding performance of the epoxy coatings on steel substrates, research efforts are focused on either reinforcing the mechanical properties of the epoxy coatings or enhancing the interfacial adhesion between the coatings and the substrates, or both.

A variety of nanofillers have been incorporated into polymeric materials to enhance their mechanical, electrical, and thermal properties as polymer reinforcement [12–14]. Among those nanofillers, carbon nanotubes (CNTs) with extraordinarily high tensile strength and young's modulus, are expected to be promising additives for epoxy coatings [15–17]. Research findings showed that adding a small percentage of CNTs into the epoxy coatings as additives was a potential way to improve the bonding performance of the epoxy coatings, since the CNTs reduced crack propagation within the coatings by increasing the fracture toughness [18,19]. The addition of CNTs in epoxy coatings could change the failure mode from brittle adhesion failure to more favorable cohesive failure [20,21]. However, the existing researches yielded inconsistent conclusions about the improvement on bonding strength, even with similar weight fractions of CNTs. Some studies showed that the bonding strength of 0.25% CNT-reinforced epoxy coatings was as much as 27% higher than that of pure epoxy coatings [22,23], while it was reported by other studies that the addition of CNTs did not seem to significantly affect the bonding strength, only a slight increase in bonding strength was obtained by CNT-reinforced epoxy adhesive with the same percentage [19, 24]. Thus, it is necessary to investigate why these research findings are inconsistent for the impacts of CNTs on the bonding performances of CNT-reinforced epoxy adhesive.

Specially, since the bonding strength of the epoxy coatings depends on both the properties of coating materials and the interfacial adhesion, the inconsistency in research findings may be induced by one of these factors.

Most of the previous researches focused on the influences of mechanical properties on the bonding performances of the CNT-reinforced epoxy and concluded that the bonding strength improvement was mainly due to the improvement of mechanical properties of the CNT-reinforced epoxy, such as the reduction of crack propagation and the increase of fracture toughness. However, when the interfacial adhesion is not strong enough, only a small part of the coatings contributes to the bond leading to the premature adhesive failure. Thus, only improving the mechanical properties of the coatings might be insufficient to achieve a firm bond if a reliable interfacial adhesion does not exist between the coatings and the substrates [25, 26]. However, the impact of these factors on the bonding performances of the CNT-reinforced epoxy has not been systematically investigated yet.

The surface roughness of the steel substrate is generally recognized as the most crucial parameter affecting the interfacial adhesion between the steel and the epoxy coatings. Several surface treatment methods have been applied to modify the surface roughness, such as mechanical blasting [27], chemical etching [28] and photolithography [29]. An adequate surface roughness is required for a good interfacial adhesion since increasing the surface roughness enlarges the contact area and introduces mechanical interlocking between the coatings and the substrates by strengthening the adsorption force at the interface [30,31]. Previous researches only compare the bonding performances of CNT-reinforced epoxy coatings with or without a certain surface treatment method [29,32,33]. It still lacks investigations on the bonding performance with a wide roughness range using the same surface treatment method, since different roughness made from different treatment methods might also contribute to the inconsistent results mentioned previously. Moreover, literatures only focused on the bonding strength to evaluate the bonding performances of the epoxy coatings, very few studies have discussed the fracture strain, which is also an important parameter for the bonding performance of the epoxy coating reflecting the coating deformability.

To address the limitations and inconsistency of previous researches on the bonding performances of the CNT-reinforced epoxy coating, for the first time as to the authors' knowledge, this paper systematically investigated the bonding performances of CNT-reinforced epoxy coatings on steel substrates with four different surface roughnesses using the single lap shear (SLS) tests. In addition to the traditional bonding performance using the bonding strength, for the first time, the fracture elongation of the coatings was also considered for bonding performance analysis. The surface morphology of the substrate before and after fracture was characterized using the scanning electron microscopy (SEM) image analysis to understand the reinforcing mechanisms of CNTs, and the wettability of water, pure epoxy and CNT-reinforced epoxy droplets on four different substrates was also measured by the contact angle tests to evaluate the interfacial adhesion of each material on each surface roughness. For the first time to the authors' knowledge, based on the experimental results, this paper clearly indicated that CNT addition could strengthen the interfacial adhesion between the coating matrix and the substrate. In addition, a statistical analysis was performed on the experimental data to estimate the bonding strength and ultimate strain of CNT-reinforced epoxy coatings under various different surface roughnesses. Although the estimation may not be universal valid, it may provide some useful information on the bonding performances of CNT-reinforced epoxy coatings with any other surface roughness that was not tested in this study to cover a wide roughness range.

2. Experimental Setup

2.1. Materials

The steel substrate was made of low carbon A36 steel (supplied by Mid America Steel Inc), which is the most common structural steel in civil and transportation applications. Both pure epoxy and CNT-reinforced epoxy coatings were prepared to compare their bonding performances. The epoxy coating matrix used in this study was mixed thoroughly using the bisphenol A based resin and the polyamide curing agent (provided by East Coast Resin) with a mixing ratio of 1:1. For the CNT-reinforced epoxy coatings, multiwalled carbon nanotubes with purity higher than 95%, diameter ranging from 50 nm to 100 nm, and length ranging from 5 μm to 20 μm length (supplied by Skyspring Nanomaterials Inc.) were used as CNTs reinforcement to modify the epoxy coatings. For the weight fraction of CNTs in the epoxy coatings, literatures showed that the bonding strength of CNT-reinforced epoxy coatings would increase with higher CNTs weight fraction till a certain percentage followed by a decrease after that [34], and 0.75% by weight to the epoxy matrix was found to be the optimal CNTs percentage [33,35]. Therefore, in this paper, to fabricate the CNT-reinforced epoxy coatings, 0.75% CNTs by weight were added into the epoxy and the mixture was mechanically stirred for 5 min, followed by ultrasonic mixing for 15 min to better disperse the CNTs into the epoxy matrix.

2.2. Surface preparation

Four different surface roughness levels were prepared to investigate their influences on bonding performances, including the smooth, fine, medium, and coarse surface conditions. Since it was reported that mechanical treatment methods can quantitively adjust the surface roughness of the substrate [36], in this paper, mechanical treatment methods using sandpaper grinding and grit blasting were applied to create the four different levels of roughness on steel substrates. The cleanness of the substrate may seriously affect the bonding performances of the coating. To remove any potential contaminants on the steel substrates induced before or during the surface treatment process, the steel substrates were ultrasonically cleaned in pure acetone solution for 15 minutes followed by compressed air cleaning before and after any surface treatments. To create the surface roughness in the smooth condition level, sandpaper grinding with 60-grit, 120-grit, 220-grit and 400-grit was conducted on the substrates successively. To prepare the surface roughness in the fine, medium, and coarse condition levels, the steel substrates were grit blasted with 20-grit, 36-grit and 60-grit aluminum oxides with a blasting pressure of 500 kPa and a standoff distance of 150 mm.

2.3. Roughness measurements

Right after all the surface treatments, the surface roughness of the steel substrates was measured using an PCE-RT 1200 roughness tester (supplied by PCE Instruments) following the ASTM D7127-17 standard [37]. Three roughness parameters were collected to evaluate the surface roughness, including the average roughness, R_z, which is the arithmetic mean of the largest individual seam depths, the arithmetic mean roughness, R_a, which is the arithmetic mean of the absolute values of the profile deviations within the reference line, and the maximum roughness, R_t, which is the distance between the highest and the lowest points on the surface [38]. On each substrate, the roughness measurements were performed on five different locations and the final roughness values were determined by the average of these five measurements for a more statistically accurate result. In addition, the surface morphology of the substrates with different roughness levels was also studied using the SEM image analysis.

2.4. Contact angle tests

In addition, since the wettability of the steel substrates is an essential surface characterization for the bonding performance of the epoxy-based coatings, this paper also studied the wettability of the steel substrates with different surface roughness using the contact angle tests. In total, twelve different combinations of contact angle tests from four different surface roughness levels (smooth, fine, medium, and coarse conditions) and three different liquid materials (water, pure epoxy, and CNT-reinforced epoxy) were performed. Water droplets were used to estimate the surface energy which is a substantial property of different substrates, while pure epoxy resin and CNT-reinforced epoxy resin were used to evaluate their wettability on all the four different substrates. The contact angle tests were carried out by the FTA1000 Drop Shape Instrument B Frame Analyzer System (supplied by First Ten Angstroms, Inc.) following the ASTM D7334-08 standard [39]. To be statistically valid, three drops of each liquid were placed on each substrate and two angle measurements were made on each edge of the droplets within 30 seconds after depositing the droplet.

2.5. SLS tests

The bonding performances of epoxy-based coatings was studied by SLS tests. The SLS test specimens were designed according to the ASTM D1002-10 standard [40] as shown in Figure 1. Two mild steel sheets with a length of 101.6 mm, a width of 25.4 mm, and a thickness of 3.18 mm were bonded together by pure epoxy or CNT-reinforced epoxy coatings in the overlap area of 12.7 mm in length. To ensure the tensile loading direction coincided with the central line of the coating and the pure shear stress was the dominant stress state within the coating, on the other ends of the two steel sheets, steel attachments with the same thickness as the steel sheets and a length of 25.4 mm were bonded using the same coating materials and thickness as in the overlap area. The surface treatments for different roughness were only performed on the overlap area of each specimen. A previous study [41] found that the optimum epoxy thickness for epoxy coating on steel surfaces was in between 0.4 and 0.5 mm because thicker coatings may lead to weaker bonding strength and thinner coatings were prone to have excessive strength data deviation. Thus, the coating thickness in this study was controlled to be around 0.5 mm by using steel shims. The two epoxy-based coating materials were applied on both surfaces of the steel sheets and assembled within 24 hours after surface treatments, followed by a 24-hour curing at 32 °C and a curing for 7 days at room temperature before the SLS tests.

Table 1 shows the test matrix for SLS tests. Eight testing groups were prepared, including two different coating materials (both pure epoxy and CNT-reinforced epoxy coatings) and four different surface roughness (smooth, fine, medium, and coarse levels). For each testing group, five valid specimens were made, resulting in a total of 60 specimens. All the SLS specimens were tested using the MTS Flex Test® SE loading frame as shown in Figure 2 under monotonic tensile loading till failure. The SLS tests were conducted by the displacement control mode at a loading rate of 1.3 mm/min. The real-time tensile load and displacement of each specimen as well as corresponding load-displacement curves were recorded. It should be noted that the tensile displacement of the specimen was equal to the elongation of the epoxy-based coatings. To calculate the bonding strength and ultimate strain of the epoxy-based coatings, the recorded tensile load and displacement were converted into shear stress and strain, so the load-displacement curves could be transformed into the stress-strain curves. For the convenience of comparison among different testing groups, the stress-strain curves of five individual specimens in one testing group were fitted mathematically into one average representative curve using the Trace Interpolation algorithm. The shape of the fitted curve was precisely similar to the five experimental curves and each point on the fitted curve was within a certain tolerance from the experimental curves. Moreover, the SEM images were also taken on the fracture surfaces of SLS specimens after testing.

3. Experimental Results

3.1. Surface characterizations

Table 2 shows the results of the average roughness (R_z, R_a and R_t) as well as its standard deviations (STDs) for the four different surface roughness levels. The STDs in percentage were calculated as the fraction of STDs by the average values. As expected, the surface roughness increased remarkably with higher roughness levels which were resulted from smaller girt size, and the same trend was seen in all the three parameters. Since the R_z and R_t only consider the characteristics of the peaks and valleys on the substrate, and the R_a gives a more comprehensive description of the profile including the height of every single point on the substrate as a commonly used international roughness parameter. Although all the three surface roughness parameters were recorded, in following discussions and analysis of this paper, only R_a was used to represent the surface roughness. Thus, the average surface roughness of the four different roughness levels of smooth, fine, medium, and coarse conditions achieved in this study, were 0.231 μm, 3.528 μm, 5.272 μm, and 8.457 μm, respectively.

The surface characterizations of the steel substrates can also be observed visually by surface morphology from the SEM analysis. Figures 3(a ~ d) show the SEM images of the four roughness levels at a magnification of 100X. The ground surface at the smooth roughness level was observed to be remarkably flat with minor interfacial scratches. The surface of the substrate at the fine level of roughness was densely filled with small bumps and holes, while at the medium roughness level the surface was majorly full of small irregularities except a few higher hills and deeper valleys and the coarse surface was clearly filled with more clearly visible hills and valleys. Higher bumps and deeper holes magnified the height difference of the profile leading to higher value of R_z and R_a, and denser distribution of these irregularities shorten the distance between peaks and bottoms resulting in smaller R_t, which verified the results of quantitative roughness measurement in Table 2.

For the wettability test results from the contact angle tests, Figures 4(a ~ d) show the typical appearances and contact angles of water droplets on four substrates with different roughness. Although all the four contact angles were less than 90º, indicating that all four substrates belonged to hydrophilic surfaces, the variation of the contact angles with four surface roughness levels shared the same trend as the roughness values increased. The contact angle of the smooth substrate was 74.72º which was apparently larger than those on the other substrates. Contact angles were noticed to be reduced from fine to medium and coarse substrates, of 59.84º, 55.67º and 48.11º, respectively. A smaller contact angle of water droplets with higher surface roughness indicated a higher wettability. Since the rougher substrates could have higher surface energy and more contact areas for the coating materials to contact with, epoxy-based coatings on rougher substrates were expected to have better bonding performance than on smoother substrates.

3.2. SLS test results

Figures 5(a, b) plot all the average stress-strain curves of pure and CNT-reinforced epoxy coatings with regard to the four different surface roughness. Figure 5(a) shows that the stress and strain of pure epoxy coatings exhibited evident linear relationship until a sudden failure occurred at the peak stress, regardless of the surface roughness levels. As for the CNT-reinforced epoxy coatings, similar to those of pure epoxy coatings, the stress-strain curves went up approximately linearly before peak stress. But after the peak stress, only the curves of smooth surfaces followed the same pattern as the pure epoxy coatings ended with a sudden failure. The curves of the rest three rougher surfaces dropped gradually from the peak stress to the failure, indicating an obvious nonlinear behavior. The three curves of CNT-reinforced epoxy coatings on the rougher surfaces showed typical stress-strain relation as for ductile materials with strain continually growing at a relatively stable stress level rather than a sharp failure for brittle materials. The nonlinearity illustrated in the curves was an indication of the plastic behavior of the epoxy coating with the addition of CNTs on the rougher steel substrates.

The average bonding strength and fracture elongation were compared in details as shown in Table 3 for all eight testing groups. The bonding strengths of the coatings were determined as the peak shear stresses from the stress-strain curves and the fracture elongations of the coatings were reflected by the ultimate strains, which was identified as the strains when the curve experienced a rapid stress drop. As shown in Table 3, almost all the STDs in one testing group were smaller than 10% for both bonding strength and ultimate strains, suggesting the consistency of the SLS tests.

4. Data analysis and discussion

4.1 Influences of the addition of CNTs in epoxy coatings

Figures 6(a, b) illustrate the bar chart comparison of bonding strength and ultimate strain between the pure and the CNT-reinforced epoxy coatings. The addition of CNTs (0.75%) showed greatly improvements of boning performances in both the bonding strength and ultimate strain, but the improvements varied with different surface roughness levels. On the smooth substrate, compared to pure epoxy, the addition of CNTs increased the bonding strength and ultimate strain by around 56% and 84%, while on the fine surfaces, while the enhancements of bonding strength and ultimate strain by adding CNTs were much more significant by around 123% and 382%, respectively. On the medium and coarse substrates, the enhancement of bonding strength by CNTs were around 70% compared to pure epoxy, but the CNTs reinforcement in epoxy improved the ultimate strain significantly by around 280%. It is also worth mentioning that the increments in ultimate strain were much more pronounced than those in bonding strength, which was largely due to the plastic deformation created by CNT-reinforced epoxy coatings.

Figure 6(c) demonstrates the toughness of the pure and the CNT-reinforced epoxy coatings with the four different surface treatments. The toughness is defined as the ability of deforming plastically and absorbing energy before fracture, which could be evaluated by the area under the stress-strain curve as in Figure 3. From Figure 6(c), it can be seen that the CNTs in epoxy only increased the toughness slightly on the smooth substrate, but greatly on the other three rougher substrates. As a result of higher toughness, the CNT-reinforced epoxy coatings generated more plastic deformation resulting in higher increases in ultimate strain and smaller increases in bonding strength, compared to pure epoxy.

Figures 7(a, b) illustrate the typical fracture surfaces of SLS specimens with or without CNTs on the smooth substrates. No obvious differences were observed on the fracture surfaces between the pure and the CNT-reinforced coatings on the smooth substrates. Both coatings had fractures occurred at the coating-substrate interfaces with all the coatings attached on the bottom surfaces of the specimens and no visible epoxy remaining on the other side, indicating a typical adhesive failure. For an adhesive failure, the interfacial adhesion instead of the coating mechanical properties played the dominating role for the bonding performance. Only the coatings near the coating-substrate interface contributed to the bond, while the rest large part of the coatings did not contribute a lot to the bond before the catastrophic failure occurred on the interface. Therefore, on the smooth substrates, increasing the mechanical properties of the epoxy-based coatings (such as toughness) by adding CNTs had little influences on the failure mode. Although the failure modes remained the same for both the pure epoxy and CNT-reinforced epoxy on smooth substrates as indicated in Figure 7, the bonding strengths and ultimate strains of the CNT-reinforced epoxy coatings on smooth surfaces were still moderately improved compared to the pure epoxy coatings as shown in Figure 6(a, b). The resulted increases on the bonding performance might be benefited from the improvement of the interfacial adhesion between the coatings and the substrates with the addition of the CNTs.

To study the CNTs contributions to the interfacial adhesion between the epoxy-based coatings and steel substrates, Figures 8(a ~ h) display the contact angles of the pure and the CNT-reinforced epoxy on the steel substrates with the four different surface roughness levels. The contact angles on smooth substrates decreased from 53.42º for pure epoxy coatings to 52.13 º for CNT-reinforced epoxy coatings, and similar reductions in contact angles were also observed in the other three rougher substrates, indicating a higher wettability by the CNTs reinforcement. Higher wettability by the addition of CNTs could increase the contact area between the CNT-reinforced epoxy coating and the substrate. In addition, the epoxy which flowed into the irregularities of the substrate was also reinforced by the CNTs, which enhanced the connection of the epoxy and the substrate as well. The reductions of the contact angle for the CNTs reinforcement in epoxy coatings confirmed with the findings from failure mode analysis in Figures 7(a, b) that the CNTs could improve the interfacial adhesion between the coatings and substrates, resulting in the improvements in the bonding performances as shown in Figures 6(a, b).

Figures 9(a, c) compare the overlap areas of the pure and the CNT-reinforced coatings on coarse substrates after SLS tests. For the pure epoxy coatings, similar as the fracture surfaces on the smooth surfaces, there was no sign of epoxy left on the top surface and all the epoxy coating on the bottom surface was free of any noticeable scars or cracks as shown in Figure 9(a), indicating that the adhesive failure was the dominant failure mode on the coarse substrates as well. However, for the CNT-reinforced epoxy coatings, as shown in Figure 9(c), a main crack was found in the middle of the coating and the coating material was left on both top and bottom surfaces. As fracture occurred within the coating layer in the cracking area, partly cohesive failure was achieved on the coarse-blasted substrates with the addition of CNTs. Figures 9(b, d) further compare the SEM images of bottom surfaces in the overlap areas with the pure and the CNT-reinforced coatings on coarse substrates after testing. The fracture surface of the CNT-reinforced coatings was observed to be much rougher than that of the pure epoxy coatings, indicating a sign of more plastic deformations and consequently more fracture energy consumption with the addition of CNTs.

To further investigate the reinforcing mechanism of CNTs in epoxy coatings, the SEM analysis under higher magnifications was conducted on the fracture surface and the main crack in Figure 9(b) of the CNT-reinforced epoxy coatings, as shown in Figures 10(a ~ d). The pulling-out of CNTs as shown in Figures 10(a) and (b) was noticed as an important reinforcing mechanism, which could improve the bonding performance of the epoxy-based coatings. It required considerable energy to pull out the CNTs from the surrounding epoxy coatings, leading to the higher toughness of the CNT-reinforced epoxy coatings than the pure epoxy coatings. Figures 10(c) and (d) illustrate the CNT clusters on the main crack. Even though the weight fraction of CNTs was optimized and the ultrasonic mixing was used in mixing the CNTs in the epoxy matrix, the CNTs were still noticed to be not uniformly dispersed in the epoxy matrix with CNTs agglomerated into clusters as shown in Figure 10(c). The aggregation of CNTs was generated primly due to the high viscosity of epoxy and high surface energy of CNTs [18], which had a detrimental effect on the bonding performance. According to the literature [42], CNTs can be divided into three levels based on the unit structure, namely individual CNTs, CNT bundles (close-packed CNTs) and CNT fibers (an assembly of CNT bundles). The strength and toughness of the CNT clusters reduced significantly, as the aggregation of CNTs become larger. These CNTs clusters consisted of both CNT bundles and CNT fibers, which reduce the reinforcing mechanism of CNTs and also caused the local stress concentration. The adverse effect of CNT clusters as defects or imperfections led to the rapid growth of the main crack, which eventually restricted the improvement of CNTs on the bonding performances. On ideal condition when the CNTs are uniformly dispersed in the epoxy matrix, CNT aggregation would not produce any defects and initial voids would be all filled by CNTs. Thus, it is expected that the bonding performance of CNT-reinforced epoxy coating would get tremendously further improved if all the imperfections were eliminated within the coating layer. Thus, how to control the CNT aggregation and improve the dispersion into epoxy resin is a prospective issue, while more in-depth investigations on this aspect are beyond the scope of this study. Future efforts are needed to improve the dispersion of CNTs in the epoxy matrix to reduce the imperfections of the resulted coatings.

4.2 Influences of surface roughness for the CNT-reinforced epoxy coatings

Figure 8 showed that the increase of the surface roughness could reduce the contact angles of the CNT-reinforced epoxy, thus, improve the wettability of the substrates, resulting in improvements in the interfacial adhesion to benefit the overall bonding performances. To further investigate the influences of surface roughness on the bonding performance of the CNT-reinforced epoxy coatings, Figure 11 plots the changes of the bonding strengths and ultimate strains of the CNT-reinforced epoxy coatings with the changes of the surface roughness parameter, R_a. In general, the changing trends of the bonding strengths and ultimate strains approximately followed a logarithmic pattern as the increase of surface roughness, with both of the curves rising rapidly at lower surface roughness and then growing at a much slower rate at larger surface roughness. On the smooth substrates with the surface roughness of 0.231 μm, the bonding strengths and ultimate strains were greatly lower than the other three rougher substrates owing to the lack of interfacial adhesion. Insufficient interfacial adhesion might result in the moderate improvements in the literature. As the surface roughness increased from 0.231 μm on smooth substrates to 3.528 μm on the fine substrates, significant increases in bonding strength and ultimate strain were noted due to the improvement of the interfacial adhesion. Stronger interfacial adhesion could prevent premature adhesive failure and allow the coatings to deform plastically as demonstrated in Figures 5 and 9.

When the steel substrates were further roughened from 3.528 μm on the fine substrates to 5.272 μm on the medium substrates and 8.457 μm on the coarse substrates, the bonding strengths barely changed, but the ultimate strains increased about 20% and 11%, from fine to coarse substrates, respectively. A much less significant changes were observed for both the bonding strengths and ultimate strains, compared to changing the surface roughness from smooth to fine conditions, indicating that although the surface roughness was of vital importance to the bonding performances of the CNT-reinforced epoxy coatings, the influence was more crucial at lower roughness levels. When surface roughness was sufficient to provide a good interfacial adhesion, further increasing the surface roughness become much less effective.

To enable an estimation of bonding performances under all different surface roughness other than the values tested in this study, various fitting approaches were performed based on the obtained data in Figure 11 and Table 3. Although there were some differences between the changes of the bonding strengths and ultimate strains for the CNT-reinforced epoxy coatings, the best fitted curves of both bonding strength and ultimate strain could be expressed into a logarithmic equation as below:

$$y = a/\{1 + \exp[-k(x - x_c)]\} \quad (1)$$

in which, a is the curve's maximum value, k is the logistic growth rate or steepness of the curve, and x_c is the value of the sigmoid's midpoint. The fitted curves using Eq. (1) was also included in Figure 11. In addition, Table 6 shows the detailed fitted parameters in Eq. (1) as well as the adjusted R-squared to evaluate the goodness of the fittings. With all the R^2 being precisely close to 1 as shown in Table 6, Figure 11 also shows that all the traces of two fitting curves staying within the STDs of measured data points on original curves, indicating an effective fitting for the experimental data for future prediction use.

In addition, Figures 12(a, b) further compare the SEM images of the top fracture surfaces for the CNT-reinforced epoxy coatings on smooth and coarse substrates. On the smooth substrates, there was no epoxy on the top surface and the fracture substrate after the SLS test was very similar to the substrate before applying the coatings. However, on the coarse substrates, it was evident that some of the CNT-reinforced epoxy penetrated into the irregularities of the substrates, as the indication of mechanical interlocking. The stronger interfacial adhesion by mechanical interlocking might contribute to the improvements of the bonding performances of the CNT-reinforced epoxy coating on rougher substrates as shown in Figure 11.

5. Conclusions

This paper investigated the bonding performances of epoxy coatings with and without CNT reinforcement on mild steel substrates fabricated with four different surface roughness. According to the experimental results, the following concluding remarks could be drawn:

(1) The addition of CNTs could significantly increase the bonding strengths and ultimate strains as a result of great improvement in the toughness of the epoxy coatings. Higher ability of plastic deformation and pulling-out of CNTs with improved fracture energy consuming efficiency might be the reinforcing mechanisms when interfacial adhesion between the epoxy coatings and steel substrates was strong enough.

(2) When lacking sufficient interfacial adhesion due to low surface roughness, the bonding performance of the CNT-reinforced epoxy coatings could still be improved because the addition of CNTs could improve the interfacial adhesion as indicated by the smaller contact angles of the CNT-reinforced epoxy compared to the pure epoxy, although the improvement was less significant.

(3) The surface roughness had a positive influence on the bonding performances of the CNT-reinforced epoxy coatings by introducing mechanical interlocking to enhance the interfacial adhesion. The positive influence of surface roughness was more significant on smoother substrates when lacking sufficient interfacial adhesion. When surface roughness was sufficient to provide a good interfacial adhesion, further increasing the surface roughness become much less effective.

(4) The failure mode could only be changed from adhesive failure of the pure epoxy coatings to partly cohesive failure of the CNT-reinforced epoxy coatings on highly rough substrates due to the aggregation of CNTs even after mechanical stirring and ultrasonic mixing.

Although the bonding strengths and ultimate strains of CNT-reinforced epoxy coatings on rough substrates were satisfactory, this study also showed that it was very challenging to achieve a complete cohesive failure only with the addition of CNTs in the epoxy because the CNTs tended to aggregate together in the epoxy coatings which introduced more defects in the coatings. In the future, researches are needed to optimize the dispersion of CNTs in the epoxy coatings and eventually to further increase the bonding performances.

CRediT authorship contribution statement

Dawei Zhang: Data curation, Methodology, Formal analysis, Investigation, Writing - original draft, Writing - review & editing. **Ying Huang**: Project administration, Funding acquisition, Supervision, Writing - review & editing. **Yechun Wang**: Data curation.

Declaration of interest

The authors declare that they have no known competing financial interests or personal relationships that could have appeared to influence the work reported in this paper.

Acknowledgements

This work was supported the National Science Foundation under Grant No. CMMI-1750316. The findings and opinions expressed in this article are those of the authors only and do not necessarily reflect the views of the sponsors.

Reference

[1] Benea L, Mardare L, Simionescu N. Anticorrosion performances of modified polymeric coatings on E32 naval steel in sea water. Prog Org Coatings 2018;123:120–7. https://doi.org/10.1016/j.porgcoat.2018.06.020.

[2] Laurentiu M, Lidia B, Eliza D, Valentin D. Polymeric coatings used against marine corrosion of naval steel EN32. Key Eng. Mater., vol. 699, Trans Tech Publications Ltd; 2016, p. 71–9. https://doi.org/10.4028/www.scientific.net/KEM.699.71.

[3] Lyon SB, Bingham R, Mills DJ. Advances in corrosion protection by organic coatings: What we know and what we would like to know. Prog Org Coatings 2017;102:2–7. https://doi.org/10.1016/j.porgcoat.2016.04.030.

[4] Zhang L, Wu H, Zheng Z, He H, Wei M, Huang X. Fabrication of graphene oxide/multi-walled carbon nanotube/urushiol formaldehyde polymer composite coatings and evaluation of their physico-mechanical properties and corrosion resistance. Prog Org Coatings 2019;127:131–9. https://doi.org/10.1016/j.porgcoat.2018.10.026.

[5] Baltzis D, Orfanidis S, Lekatou A, Paipetis AS. Stainless steel coupled with carbon nanotube-modified epoxy and carbon fibre composites: Electrochemical and mechanical study. Plast Rubber

Compos 2016;45:95–105. https://doi.org/10.1080/14658011.2016.1144339.

[6] Parhizkar N, Ramezanzadeh B, Shahrabi T. Corrosion protection and adhesion properties of the epoxy coating applied on the steel substrate pre-treated by a sol-gel based silane coating filled with amino and isocyanate silane functionalized graphene oxide nanosheets. Appl Surf Sci 2018;439:45–59. https://doi.org/10.1016/j.apsusc.2017.12.240.

[7] García GL, López-Ríos V, Espinosa A, Abenojar J, Velasco F, Toro A. Cavitation resistance of epoxy-based multilayer coatings: Surface damage and crack growth kinetics during the incubation stage. Wear 2014;316:124–32. https://doi.org/10.1016/j.wear.2014.04.007.

[8] Bahlakeh G, Ramezanzadeh B. A Detailed Molecular Dynamics Simulation and Experimental Investigation on the Interfacial Bonding Mechanism of an Epoxy Adhesive on Carbon Steel Sheets Decorated with a Novel Cerium-Lanthanum Nanofilm. ACS Appl Mater Interfaces 2017;9:17536–51. https://doi.org/10.1021/acsami.7b00644.

[9] Semoto T, Tsuji Y, Yoshizawa K. Molecular understanding of the adhesive force between a metal oxide surface and an epoxy resin. J Phys Chem C 2011;115:11701–8. https://doi.org/10.1021/jp202785b.

[10] Moulds RJ, Baldwin TR. Toughened adhesives for structural applications. Int J Adhes Adhes 1983; vol. 3:203–207. https://doi.org/10.1016/0143-7496(83)90095-7

[11] Kim KS, Yoo JS, Yi YM, Kim CG. Failure mode and strength of uni-directional composite single lap bonded joints with different bonding methods. Compos Struct 2006;72:477–85. https://doi.org/10.1016/j.compstruct.2005.01.023.

[12] Lee JH, Rhee KY, Park SJ. Silane modification of carbon nanotubes and its effects on the material properties of carbon/CNT/epoxy three-phase composites. Compos Part A Appl Sci Manuf 2011;42:478–83. https://doi.org/10.1016/j.compositesa.2011.01.004.

[13] Jojibabu P, Jagannatham M, Haridoss P, Janaki Ram GD, Deshpande AP, Bakshi SR. Effect of different carbon nano-fillers on rheological properties and lap shear strength of epoxy adhesive joints. Compos Part A Appl Sci Manuf 2016;82:53–64. https://doi.org/10.1016/j.compositesa.2015.12.003.

[14] Park SM, Shon MY. Effects of multi-walled carbon nano tubes on corrosion protection of zinc rich

epoxy resin coating. J Ind Eng Chem 2015;21:1258–64. https://doi.org/10.1016/j.jiec.2014.05.042.

[15] Yu S, Tong MN, Critchlow G. Use of carbon nanotubes reinforced epoxy as adhesives to join aluminum plates. Mater Des 2010;31. https://doi.org/10.1016/j.matdes.2009.11.045.

[16] Seo DW, Lim JK. Tensile, bending and shear strength distributions of adhesive-bonded butt joint specimens. Compos Sci Technol 2005;65:1421–7. https://doi.org/10.1016/j.compscitech.2004.12.013.

[17] Khoramishad H, Khakzad M. Toughening epoxy adhesives with multi-walled carbon nanotubes. J Adhes 2018;94:15–29. https://doi.org/10.1080/00218464.2016.1224184.

[18] Razavi SMJ, Ayatollahi MR, Nemati Giv A, Khoramishad H. Single lap joints bonded with structural adhesives reinforced with a mixture of silica nanoparticles and multi walled carbon nanotubes. Int J Adhes Adhes 2018;80:76–86. https://doi.org/10.1016/j.ijadhadh.2017.10.007.

[19] Konstantakopoulou M, Kotsikos G. Effect of MWCNT filled epoxy adhesives on the quality of adhesively bonded joints. Plast Rubber Compos 2016;45:166–72. https://doi.org/10.1080/14658011.2016.1165788.

[20] Cheng F, Hu Y, Lv Z, Chen G, Yuan B, Hu X, et al. Directing helical CNT into chemically-etched micro-channels on aluminum substrate for strong adhesive bonding with carbon fiber composites. Compos Part A Appl Sci Manuf 2020;135. https://doi.org/10.1016/j.compositesa.2020.105952.

[21] Wang B, Bai Y, Hu X, Lu P. Enhanced epoxy adhesion between steel plates by surface treatment and CNT/short-fibre reinforcement. Compos Sci Technol 2016;127:149–57. https://doi.org/10.1016/j.compscitech.2016.03.008.

[22] Amitkumar R, Asokan R, Jhanji KP, Das D, Sai NV. Investigation of tensile properties of carbon/epoxy composite joints with and without carbon nano-tubes. Int J Veh Struct Syst 2019;11:209–13. https://doi.org/10.4273/ijvss.11.2.19.

[23] Han S, Meng Q, Araby S, Liu T, Demiral M. Mechanical and electrical properties of graphene and carbon nanotube reinforced epoxy adhesives: Experimental and numerical analysis. Compos Part A Appl Sci Manuf 2019;120:116–26. https://doi.org/10.1016/j.compositesa.2019.02.027.

[24] Prolongo SG, Gude MR, Ureña A. Rheological behaviour of nanoreinforced epoxy adhesives of low electrical resistivity for joining carbon fiber/epoxy laminates. J Adhes Sci Technol 2010;24:1097–

112. https://doi.org/10.1163/016942409X12584625925060.

[25] Marshall SJ, Bayne SC, Baier R, Tomsia AP, Marshall GW. A review of adhesion science. Dent Mater 2010;26. https://doi.org/10.1016/j.dental.2009.11.157.

[26] Zhang D, Huang Y. Influence of surface roughness and bondline thickness on the bonding performance of epoxy adhesive joints on mild steel substrates. Prog Org Coatings 2021;153:106135. https://doi.org/10.1016/j.porgcoat.2021.106135.

[27] Rajput A, Ak M, Kim SJ, Noh SH, Park JH, Paik JK. Effects of the surface preparation on the life of epoxy coating in steel ship plates: an experimental study. Ships Offshore Struct 2019;14:199–206. https://doi.org/10.1080/17445302.2019.1565072.

[28] Lei Y, Ma Y, Zhang B, Lei B, Li Y. Enhancement the adhesion between epoxy coating and rusted structural steel by tannic acid treatment. Acta Metall Sin (English Lett 2014;27:1105–13. https://doi.org/10.1007/s40195-014-0132-5.

[29] Gude MR, Prolongo SG, Gómez-Del Río T, Ureña A. Mode-I adhesive fracture energy of carbon fibre composite joints with nanoreinforced epoxy adhesives. Int J Adhes Adhes 2011;31:695–703. https://doi.org/10.1016/j.ijadhadh.2011.06.016.

[30] Hunter R, Ibacache N, Möller J, Betancourt R, Mora T, Diez E, et al. Influence of roughness on the mechanical adhesion of single lap joints. J. Adhes., vol. 88, 2012, p. 376–90. https://doi.org/10.1080/00218464.2012.660107.

[31] Fernando D, Teng ; J G, Asce M, Yu ; T, Zhao XL, Asce F. Preparation and Characterization of Steel Surfaces for Adhesive Bonding 2013. https://doi.org/10.1061/(ASCE)CC.1943-5614.

[32] Yun IH, Kim WS, Kim K, Jung JM, Lee JJ, Jung HT. Highly enhanced interfacial adhesion properties of steel-polymer composites by dot-shaped surface patterning. J. Appl. Phys., vol. 109, 2011. https://doi.org/10.1063/1.3567113.

[33] Kumar A, Kumar K, Ghosh PK, Rathi A, Yadav KL, Raman. MWCNTs toward superior strength of epoxy adhesive joint on mild steel adherent. Compos Part B Eng 2018;143:207–16. https://doi.org/10.1016/j.compositesb.2018.01.016.

[34] Ayatollahi MR, Nemati Giv A, Razavi SMJ, Khoramishad H. Mechanical properties of adhesively

single lap-bonded joints reinforced with multi-walled carbon nanotubes and silica nanoparticles. J Adhes 2017;93:896–913. https://doi.org/10.1080/00218464.2016.1187069.

[35] Sydlik SA, Lee JH, Walish JJ, Thomas EL, Swager TM. Epoxy functionalized multi-walled carbon nanotubes for improved adhesives. Carbon N Y 2013;59:109–20. https://doi.org/10.1016/j.carbon.2013.02.061.

[36] Sen D, Chavan NM, Rao DS, Sundararajan G. Influence of grit blasting on the roughness and the bond strength of detonation sprayed coating. J. Therm. Spray Technol., vol. 19, 2010, p. 805–15. https://doi.org/10.1007/s11666-010-9476-1.

[37] ASTM. D7127-13. Standard test method for measurement of surface roughness of abrasive blast cleaned metal surfaces using a portable stylus instrument. ASTM Int 2014:1–6. https://doi.org/10.1520/D7127-13.2.

[38] Gadelmawla ES, Koura MM, Maksoud TMA, Elewa IM, Soliman HH. Roughness parameters. J Mater Process Technol 2002;123:133–45. https://doi.org/10.1016/S0924-0136(02)00060-2.

[39] Designation: D7334 − 08 (Reapproved 2013) Standard Practice for Surface Wettability of Coatings, Substrates and Pigments by Advancing Contact Angle Measurement 1 n.d. https://doi.org/10.1520/D7334-08R13.

[40] Standard Test Method for Apparent Shear Strength of Single-Lap-Joint Adhesively Bonded Metal Specimens by Tension Loading (Metal-to-Metal) 1 2019. https://doi.org/10.1520/D1002-10R19.

[41] Arenas JM, Narbón JJ, Alía C. Optimum adhesive thickness in structural adhesives joints using statistical techniques based on Weibull distribution. Int J Adhes Adhes 2010;30:160–5. https://doi.org/10.1016/j.ijadhadh.2009.12.003.

[42] Gao E, Lu W, Xu Z. Strength loss of carbon nanotube fibers explained in a three-level hierarchical model. Carbon N Y 2018;138:134–42. https://doi.org/10.1016/j.carbon.2018.05.052.

Figure captions

Fig. 1. The detailed specimen configuration (Unit: mm)

Fig. 2. The SLS test setup

Fig. 3. SEM images of steel substrates of four roughness levels at a magnification of 100X: (a) the smooth; (b) fine; (c) medium; and (d) coarse substrates

Fig. 4. Contact angles of water droplets on four different roughness substrates: (a) the smooth; (b) fine; (c) medium; and (d) coarse substrates

Fig. 5 Average stress-strain curves with different surface roughness: (a) the pure; and (b) CNT-reinforced epoxy coatings

Fig. 6 Increments between the pure and the CNT-reinforced epoxy coatings: (a) bonding strength; (b) ultimate strain; and (c) toughness

Fig. 7 Typical fracture surfaces on smooth substrates: (a) the pure; and (b) CNT-reinforced epoxy coating;

Fig. 8. Contact angles of pure and CNT-reinforced epoxy droplets: (a) pure epoxy on the smooth substrate; (b) pure epoxy on the fine substrate; (c) pure epoxy on the medium substrate; (d) pure epoxy on the coarse substrate; (e) the CNT-reinforced epoxy on the smooth substrate; (f) the CNT-reinforced epoxy on the fine substrate; (g) the CNT-reinforced epoxy on the medium substrate; and (h) the CNT-reinforced epoxy on the coarse substrate;

Fig. 9 Typical fracture surfaces on coarse substrates: (a) pure epoxy coating; (b) SEM image of the fractured pure epoxy coating at a magnification of 500X; (c) the CNT-reinforced epoxy coating; (d) SEM image of the fractured CNT-reinforced epoxy coating at a magnification of 500X;

Fig. 10 Detection of CNTs: (a) on fracture surfaces at a magnification of 5000X; (b) on fracture surfaces at a magnification of 10,000X; (c) on the main crack at a magnification of 500X; (d) on the main crack at a magnification of 10,000X;

Fig. 11 Changes of bonding strength and ultimate strain of the CNT-reinforced epoxy coatings with different surface roughness

Fig. 12 Typical fracture surfaces of the CNT-reinforced epoxy coating on top surfaces at a magnification of 500X: (a) on the smooth substrate; (b) on the coarse-blasted substrate;

Table 1. The SLS test matrix

Testing group	Specimen quantity	Surface roughness	Coating thickness	Coating material
SE	5	Smooth	0.5 mm	Epoxy
FE	5	Fine	0.5 mm	Epoxy
ME	5	Medium	0.5 mm	Epoxy
CE	5	Coarse	0.5 mm	Epoxy
SC	5	Smooth	0.5 mm	CNT-reinforced epoxy
FC	5	Fine	0.5 mm	CNT-reinforced epoxy
MC	5	Medium	0.5 mm	CNT-reinforced epoxy
CC	5	Coarse	0.5 mm	CNT-reinforced epoxy

Table 2. Average measured roughness results for four different surface treatments

Roughness level	Grit size	R_z (μm)	STD (%)	R_a (μm)	STD (%)	R_t (μm)	STD (%)
Smooth	60, 120, 240, 400	1.801 ± 0.014	7.77	0.231 ± 0.017	7.36	2.044 ± 0.204	9.98
Fine	60	23.72 ± 1.76	7.42	3.528 ± 0.164	4.64	27.17 ± 2.48	9.13
Medium	36	36.13 ± 0.19	0.53	5.272 ± 0.343	6.51	35.51 ±1.98	5.58
Coarse	20	46.07 ± 4.17	9.05	8.457 ± 0.737	8.71	48.28 ± 2.91	6.03

Table 3. The SLS test results

Group	Surface roughness, R_a (μm)	Bonding strength (MPa)	STD (%)	Ultimate strain	STD (%)
SE	0.231	9.455± 0.699	7.39	0.534 ± 0.042	7.87
FE	3.528	12.234 ±0.765	6.25	0.692 ± 0.059	8.53
ME	5.272	14.764 ± 0.801	5.43	0.766 ± 0.068	8.88
CE	8.457	15.145 ± 0.776	5.12	0.805 ± 0.081	10.00
SC	0.231	11.595 ± 0.204	1.76	0.607 ± 0.031	5.11
FC	3.528	18.573 ± 0.409	2.20	1.416 ± 0.042	2.97
MC	5.272	19.475 ± 0.545	2.80	1.702 ± 0.100	5.88
CC	8.457	20.057 ± 1.053	5.25	1.876 ± 0.117	6.24

Table 4. Parameter values for each curve

	Parameter value: a	Parameter value: Xc	Parameter value: k	R2
Strength	19.992	-0.244	0.679	0.999
Strain	1.928	1.656	0.546	0.999

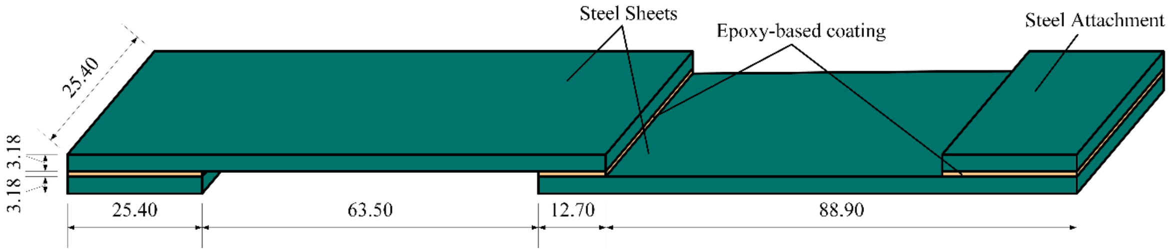

Fig. 1. The detailed SLS specimen configuration (Unit: mm)

Fig. 2. The SLS test setup

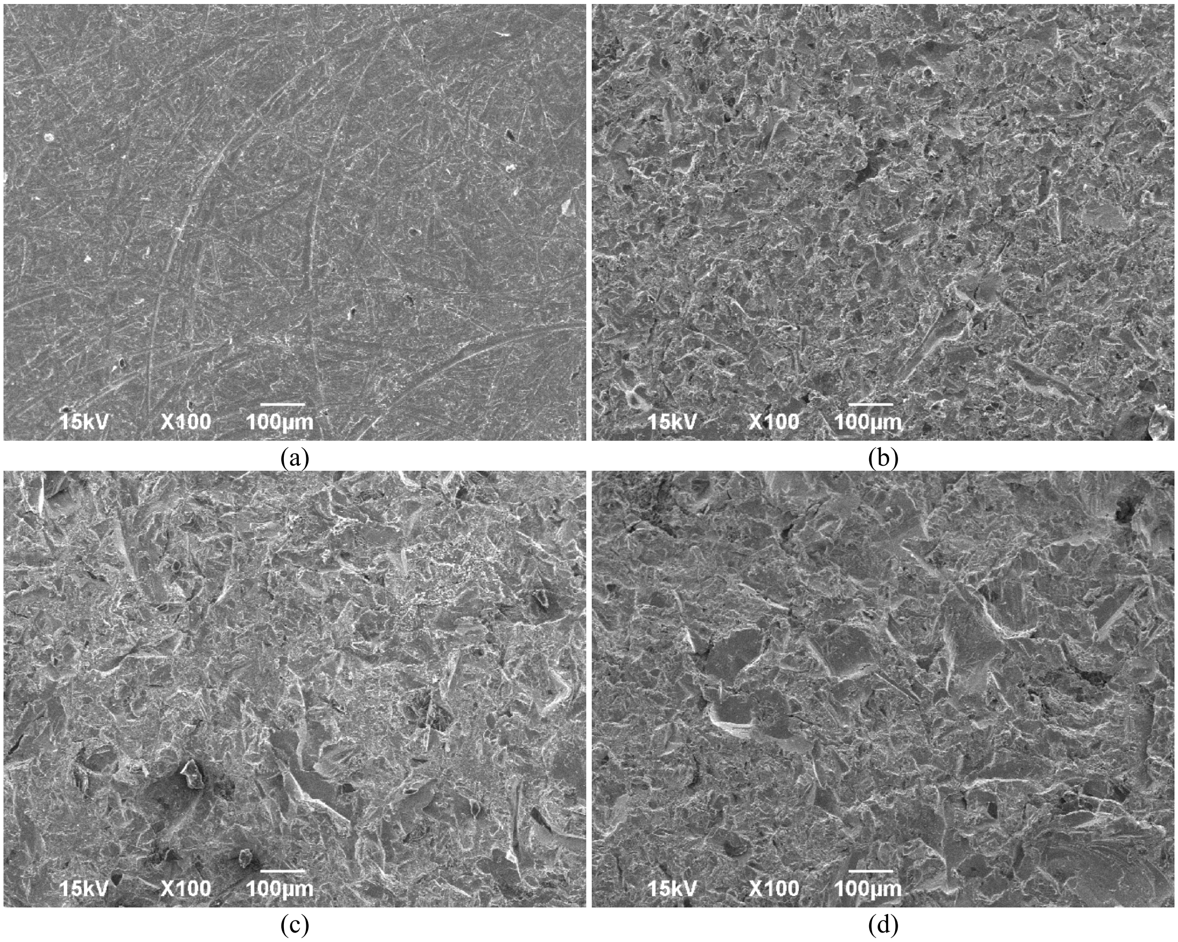

Fig. 3. SEM images of steel substrates of four roughness levels at a magnification of 100X: (a) the smooth; (b) fine; (c) medium; and (d) coarse substrates.

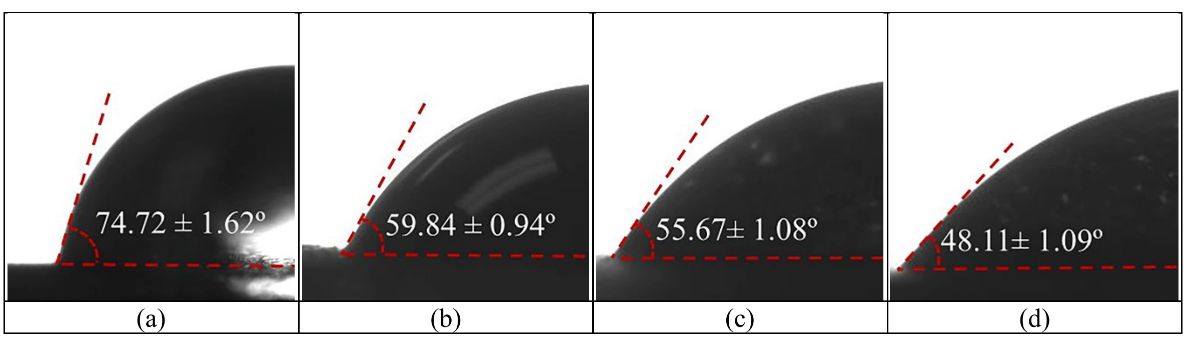

Fig. 4. Contact angles of water droplets on four different roughness substrates: (a) the smooth; (b) fine; (c) medium; and (d) coarse substrates.

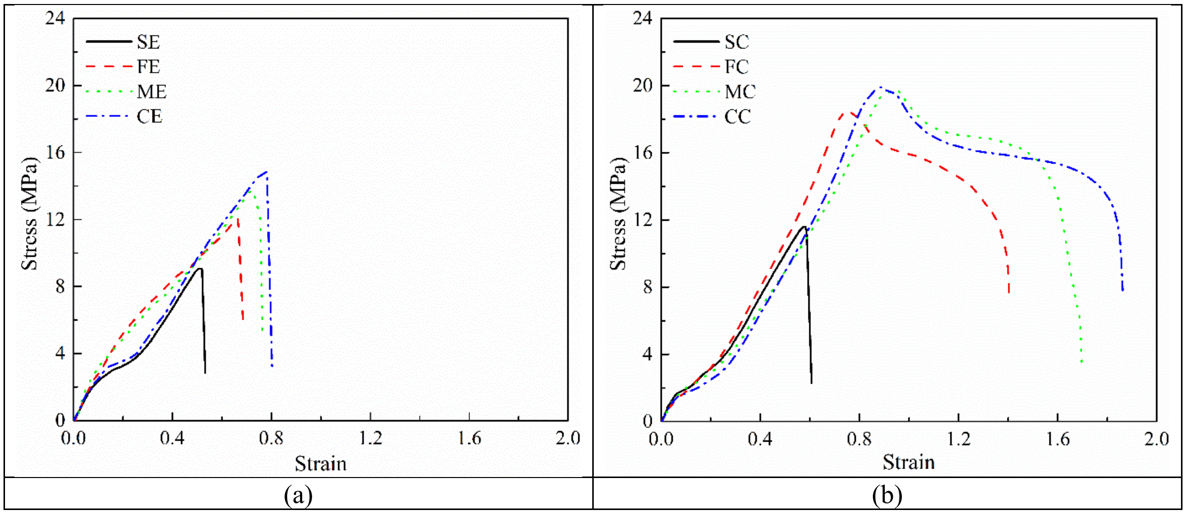

Fig. 5 Average stress-strain curves with different surface roughness: (a) the pure; and (b) the CNT-reinforced epoxy coatings.

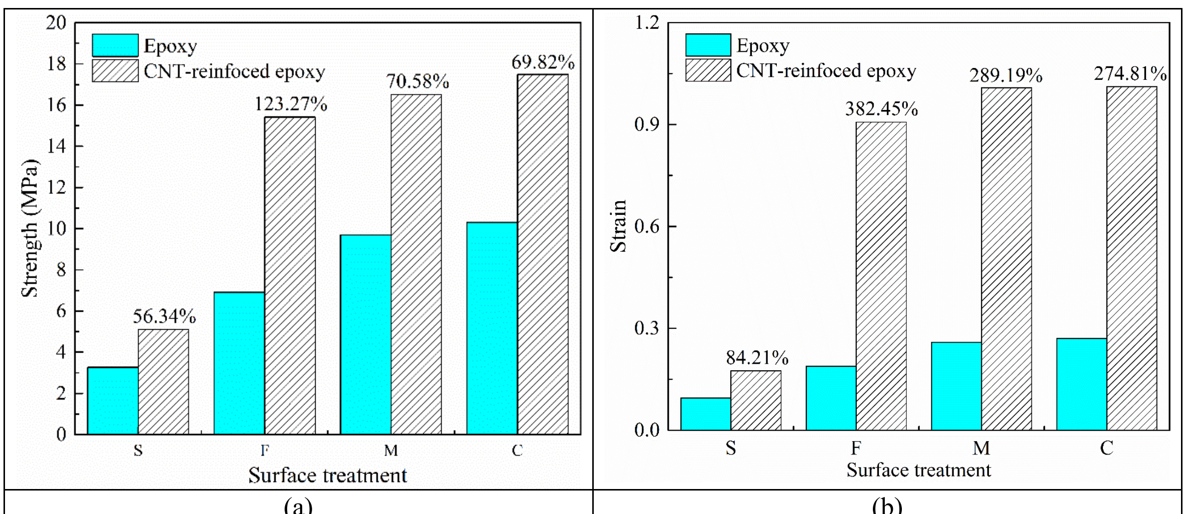

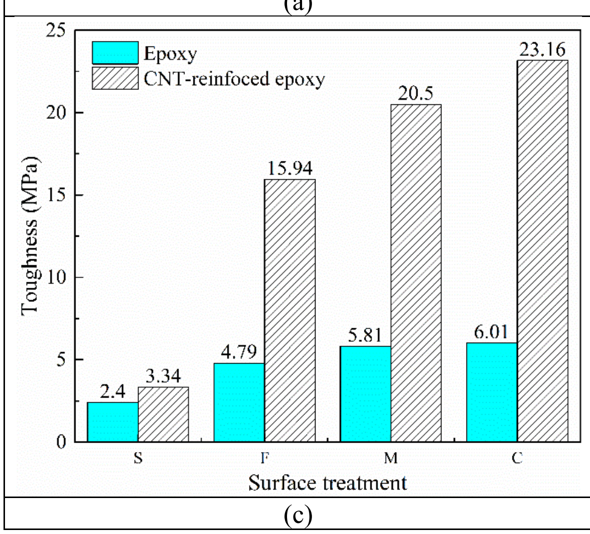

Fig. 6 Increments between the pure and the CNT-reinforced epoxy coatings: (a) bonding strength; (b) ultimate strain; and (c) toughness.

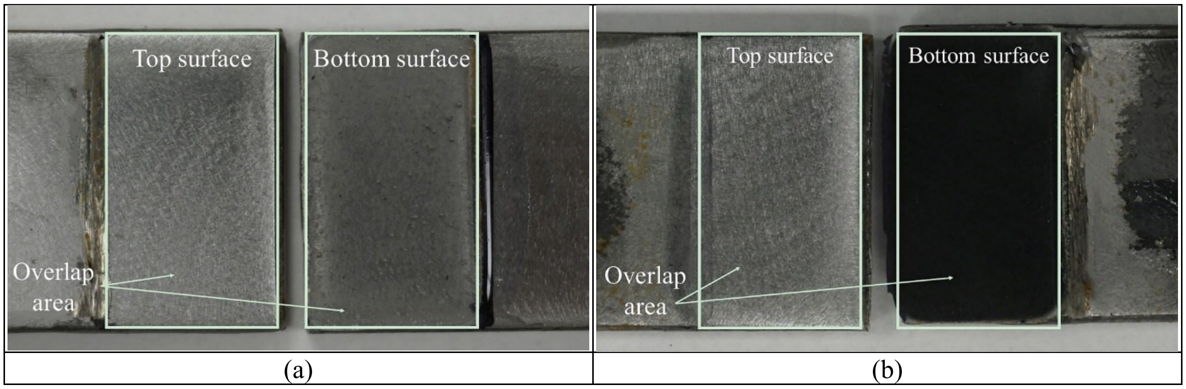

Fig. 7 Typical fracture surfaces on smooth substrates: (a) the pure; and (b) the CNT-reinforced epoxy coating.

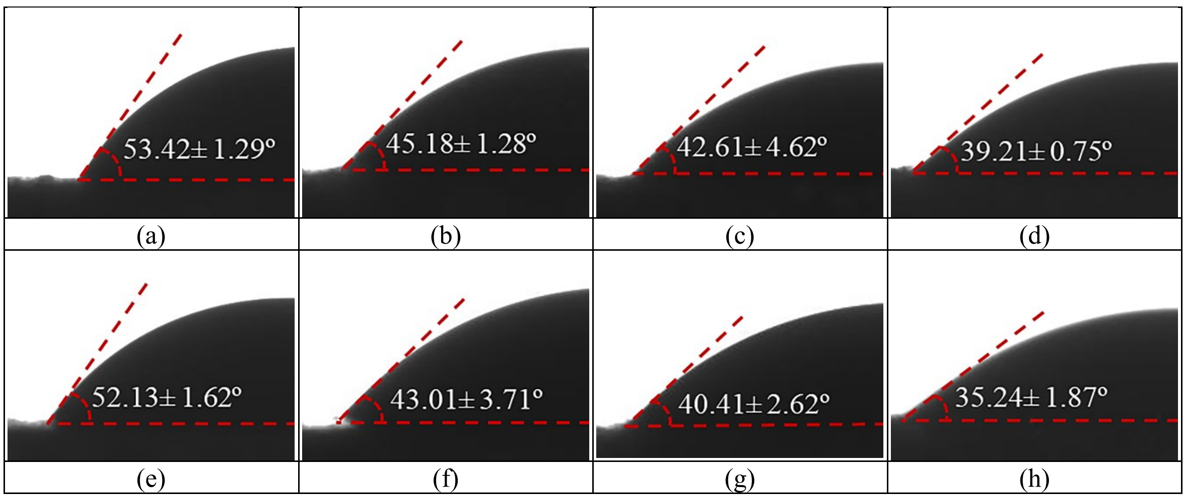

Fig. 8. Contact angles of the pure and CNT-reinforced epoxy droplets: (a) pure epoxy on the smooth substrates; (b) pure epoxy on the fine substrates; (c) pure epoxy on the medium substrates; (d) pure epoxy on the coarse substrates; (e) the CNT-reinforced epoxy on the smooth substrates; (f) the CNT-reinforced epoxy on the fine substrates; (g) the CNT-reinforced epoxy on the medium substrates; and (h) the CNT-reinforced epoxy on the coarse substrates.

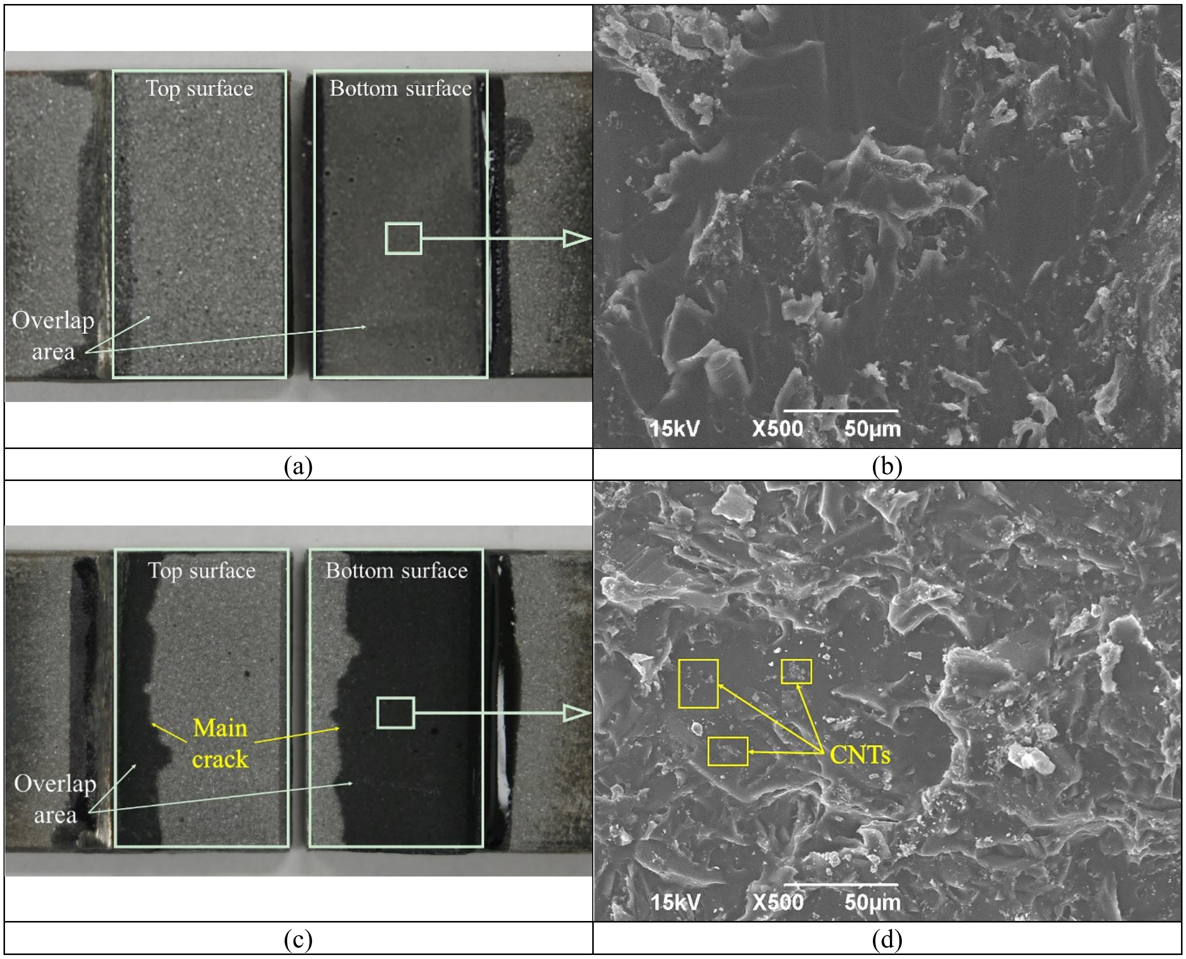

Fig. 9 Typical fracture surfaces on coarse substrates: (a) pure epoxy coating; (b) SEM image of the fractured pure epoxy coating at a magnification of 500X; (c) the CNT-reinforced epoxy coating; (d) SEM image of the fractured CNT-reinforced epoxy coating at a magnification of 500X.

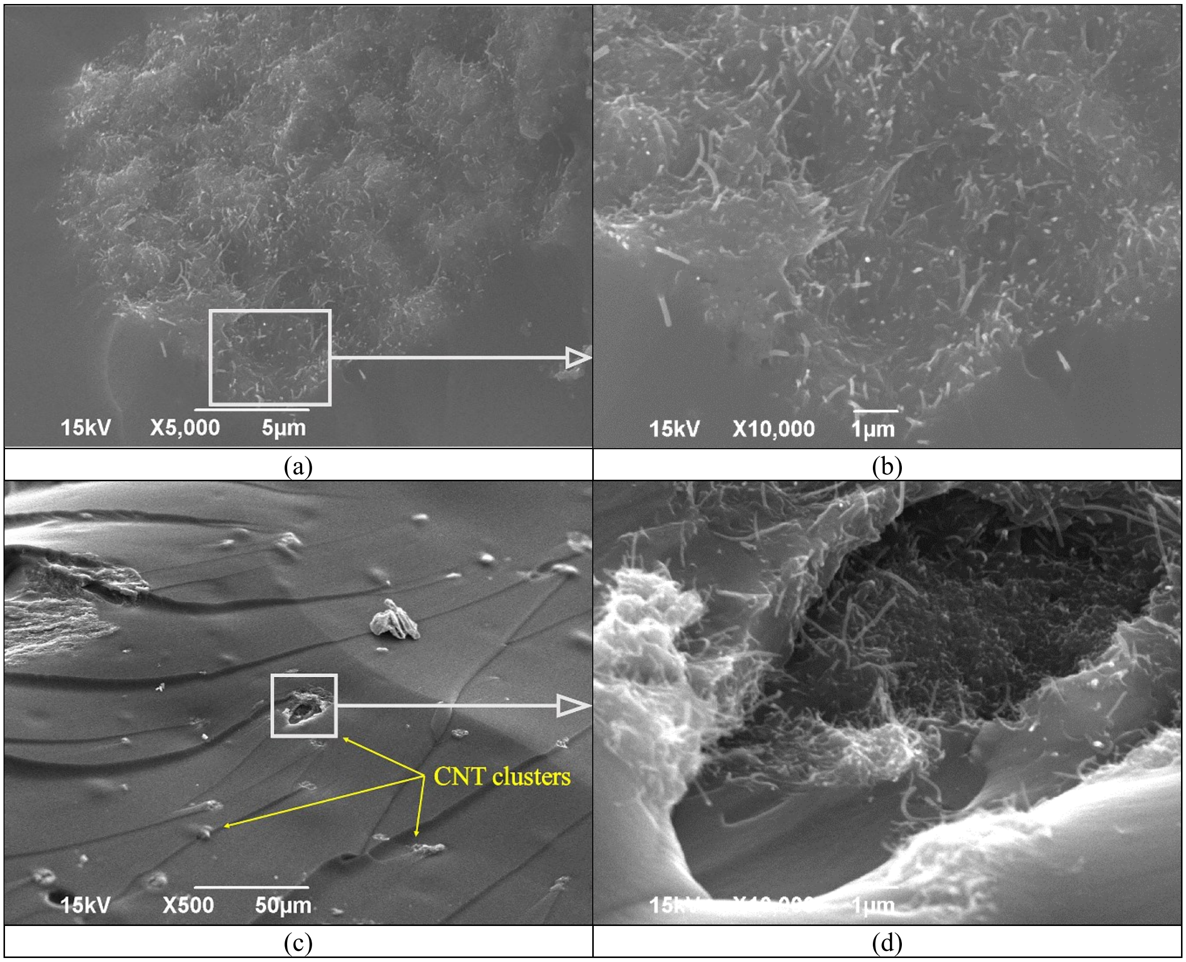

Fig. 10 Detection of CNTs: (a) on fracture surfaces at a magnification of 5000X; (b) on fracture surfaces at a magnification of 10,000X; (c) on the main crack at a magnification of 500X; (d) on the main crack at a magnification of 10,000X;

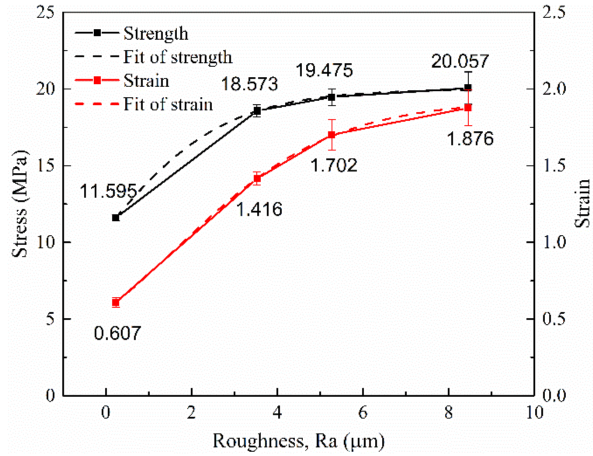

Fig. 11 Changes of bonding strengths and ultimate strains of the CNT-reinforced epoxy coatings with different surface roughness

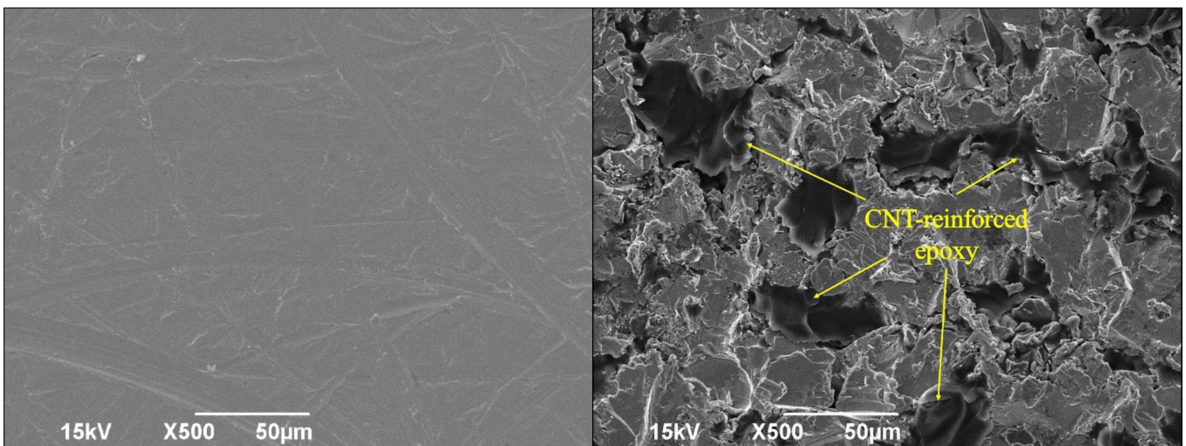

(a)	(b)

Fig. 12 Typical fracture surfaces of the CNT-reinforced epoxy coating on top surfaces at a magnification of 500X: (a) on the smooth substrate; (b) on the coarse-blasted substrate;